JOURNAL OF THERMOPHYSICS AND HEAT TRANSFER
Vol. 16, No. 3, July–September 2002

Response of Heatshield Material at Stagnation Point of Pioneer-Venus Probes

Hyo-Keun Ahn,* Chul Park,† and Keisuke Sawada‡
Tohoku University, Sendai 980-77, Japan

The ablation, pyrolysis gas formation and removal, and heat conduction phenomena at the stagnation point of the heatshield for the four Pioneer-Venus probe vehicles are calculated. The motion of the pyrolysis gas is calculated by solving the mass and momentum equations for the gas, accounting for friction and inertial forces. The developed computer code gives satisfactory results when applied to two ground-based cases and one flight-test case. For the calculation of the Pioneer-Venus flight cases, recently calculated values of convective and radiative heating rates are used. Good agreement is seen in thermocouple temperature for the day probe and north probe for which the entry angle and flight trajectory are known. For the night probe and large probe, for which entry angle and flight trajectory are unknown, agreement is poor.

Nomenclature

B = activation temperature, K
c_p = specific heat, $J \cdot kg^{-1} \cdot K^{-1}$
d = thickness of heatshield, m
e = internal energy, J/kg
f = friction force per unit volume, N/m^3
K = permeability, m^2
M = mass of entry body, kg
p = pressure
R = pyrolysis rate, $kg \cdot m^{-3} \cdot s^{-1}$
R_N = nose radius, m
s = distance along surface from stagnation point, m
T = temperature, K
t = time, s
u = velocity, m/s
x = distance from inner boundary, m
γ = flight angle, deg
ε = void fraction
κ = conductivity, $W \cdot m^{-1} \cdot K^{-1}$
μ = viscosity, $N \cdot s/m^2$
ρ = density, kg/m^3
ρ_p = intrinsic density of phenolic resin, kg/m^3

Subscripts

c = char
g = pyrolysis gas
i = inner boundary
j = index for computational node
r = resin
s = solid
v = virgin
w = wall

Received 4 April 2001; revision received 1 April 2002; accepted for publication 2 April 2002.

*Graduate Student, Department of Aeronautics and Space Engineering; currently Research Engineer, Aerodynamics Division, Mail Stop 3-2-1, Agency for Defense Development, P.O. Box 35-3, Yuseong-ku, Taejon 305-600, Republic of Korea; ahklee@hanmail.net.

†Professor, Department of Aeronautics and Space Engineering; currently Senior Research Scientist, Space Technology Division, Mail Stop 230-2, NASA Ames Research Center, Moffett Field, CA 94035; cpark@mail.arc.nasa.gov. Fellow AIAA.

‡Professor, Department of Aeronautics and Space Engineering; sawada@cfd.mech.tohoku.ac.jp. Associate Fellow AIAA.

Introduction

IN 1978, four probe vehicles, named day probe, north probe, night probe, and large probe, entered the atmosphere of Venus at a nominal entry speed of 11.5 km/s (Ref. 1). The vehicle had a sphere–cone geometry with a cone half-angle of 45 deg. The vehicles were thermally protected by a heatshield made of carbon–phenolic. At or near the stagnation point and at a point close the frustum edge on all of these four vehicles, a thermocouple had been imbedded at a depth of 3–4 mm. All thermocouples functioned, and the temperature histories of all of these thermocouples have been received. Entry angles for these four vehicles ranged from about −25 to −70 deg. For the day probe and north probe, the accelerometers functioned also. From the accelerometer data, the trajectories of these two vehicles have been reconstructed. For the other two probes, the intended entry angles are known, but the actual entry angles or their flight trajectories are unknown because the accelerometers did not function.

In 1980, Wakefield and Pitts[2] attempted to numerically reconstruct the thermocouple data for the day probe and north probe using the materials response code charring materials ablation (CMA).[3] They used the then best available calculated values of the combined convective and radiative heating rates.[4,5] The calculated thermocouple temperature values rose to unrealistically high values for both the stagnation point and the frustum edge.

Recently, Park and Ahn[6] reevaluated the convective and radiative heating rates for the four probes at the stagnation point. Their heating rate values are substantially lower than the values used by Wakefield and Pitts.[2]

It is the purpose of the present work to reevaluate the material response of the Pioneer-Venus vehicles using the newly derived heating rate values of Park and Ahn.[6] The calculated thermocouple temperature values are compared with the flight data.

When the present calculation of material response for the Pioneer-Venus vehicles is carried out, one modification is made to the CMA code used by Wakefield and Pitts.[2] The CMA code used by Wakefield and Pitts assumes that the flow of the pyrolysis gas produced within the heatshield material is in a steady state even though the rate of advance of the pyrolysis zone is different from that of the receding surface. This assumption eliminates the need to solve for the motion of the pyrolysis gas inside the material. However, because of the relatively steep entry angles, the heating pulses for those vehicles were sudden and, therefore, it is not a priori evident that this assumption of steady-state pyrolysis gas flow is valid for the Pioneer-Venus probes.

The method of treating the motion of the pyrolysis gas has been studied beginning in the 1960s.[7–11] The method is implemented in the present work in a form suitable for computational fluid dynamic (CFD) calculation. The permeability of ablative materials, which must be specified in calculating the motion of pyrolysis gas, is known for some materials.[12–14] The present work uses interpolation of the existing data to estimate the permeability values for the Pioneer-Venus vehicles.

The modified CMA code, Super CMA (SCMA), is first applied to two laboratory conditions. Good agreement is found between the calculated and measured surface temperatures. Comparison is made also against an alternate method of computing the materials response, the heat balance integral (HBI)[15] method, for a flight-test case. The treatment of physical phenomena in the HBI method is the same as in CMA, except that the thickness of the pyrolysis zone is assumed to be infinitesimally small. Good agreement is also found here.

The results of the present work for the Pioneer-Venus vehicles show that the thermocouple temperatures calculated for the day probe and north probe agree with the flight data, although the onset of the temperature rise is earlier by about 2 s. The possible reason for the 2-s discrepancy is surmised. For the night probe and large probe, for which the entry angle and flight trajectory are unknown, the calculated thermocouple temperatures are higher than the flight data, and the onset of the temperature rise is earlier by about 5 s.

Governing Equations

For planetary entries, the body dimensions are much larger than the thickness of the heatshield. As a result, the ablation phenomenon can be safely considered to be one-dimensional. Also, the rate of ablation is much smaller than the velocity of the pyrolysis gas. Therefore, the recession of the surface is ignored in the governing equations for the pyrolysis gas. Recession is accounted for by redrawing the coordinates after each time step. The temperature of the pyrolysis gas is taken to be the same as the temperature of the solid at the given position.

The dependent variables of the problem are solid density ρ_s, gas density ρ_g, pyrolysis gas velocity u, solid internal energy per unit mass e_s, gas internal energy per unit mass e_g, and temperature T. The solid quantities are divided into those of char and resin, that is, ρ_c vs ρ_r and e_c vs e_r, respectively. Resin density is the difference between the solid and char densities. The void fraction ε is related to the char density and solid density by

$$\varepsilon = \varepsilon_{\max} + (\rho_c - \rho_s)/\rho_p \tag{1}$$

where $\varepsilon_{\max}$ is the maximum value in the char state and ρ_p is the intrinsic density of the resin. McManus and Springer[8] studied thermomechanical behavior of carbon–phenolic and carbon–carbon composites. The quantities $\varepsilon_{\max}$ and ρ_p are deduced from that work using the data in Ref. 2 as $\varepsilon_{\max} = 0.1788$ and $\rho_p = 1763.6$ kg/m^3. Then the governing equations become

$$\frac{\partial \rho_r}{\partial t} = -R \tag{2}$$

$$\frac{\partial}{\partial t}(\varepsilon\rho_g) + \frac{\partial}{\partial x}(\varepsilon\rho_g u) = R + D \tag{3}$$

$$\frac{\partial}{\partial t}(\varepsilon\rho_g u) + \frac{\partial}{\partial x}\left(\varepsilon\rho_g u^2 + \varepsilon p\right) = -\varepsilon f + I \tag{4}$$

$$\frac{\partial}{\partial t}\left(\rho_c e_c + \rho_r e_r + \varepsilon\rho_g e_g + \frac{1}{2}\varepsilon\rho_g u^2\right) + \frac{\partial}{\partial x}\left[\varepsilon u\left(\rho_g e_g + \frac{1}{2}\rho_g u^2 + p\right)\right] = \frac{\partial}{\partial x}\left(\kappa\frac{\partial T}{\partial x}\right) \tag{5}$$

The four equations are for solid mass, gas mass, gas momentum, and total energy conservation, respectively. Here p and f are the pressure and friction force of the pyrolysis gas, respectively. D is the rate of change of pyrolysis gas density by diffusion, and I is inertial force.

Friction Force

The friction force is obtained from the empirical relationship between velocity of the flow and permeability in a steady flow[16]:

$$f = (\mu/K)u \tag{6}$$

To obtain the viscosity of the pyrolysis gas, the equilibrium composition of the pyrolysis gas is examined in the temperature range from 500 to 4000 K and pressure range from 1 to 10 atm. To within an accuracy of 0.1%, the pyrolysis gas is found to consist of H, H_2, CO, and CH_4. The pyrolysis gas is considered to be a mixture of two components: component 1 consisting of the H–H_2–CO mixture and component 2 consisting of CH_4. The viscosity of the first component is calculated using the collision integrals given in Ref. 17 and using Eq. (4.35) in Ref. 18. The viscosity of the second component is taken from Ref. 19. These two viscosity values are combined through the use of the mixture rule[20] to obtain the viscosity of the whole mixture. The resulting viscosity values are fitted by

$$\mu = 2.525 \times 10^{-5}(T/500)^{0.769} \tag{7}$$

Recently, experiments for gas permeability of thermal protection materials were conducted. Marschall and Milos[21] demonstrated in their experiment that the pressure dependence of gas permeability can be represented by the Klinkenberg formulation and expressed the effective permeability in the form

$$K = K_0(1 + b/p) \tag{8}$$

where K_0 is the gas permeability in the limit of continuum flow and b is permeability slip parameter. From the experimental results of Marschall and Cox[14] for phenolic impregnated carbon ablator (PICA) and silicone impregnated reusable ceramic ablator (SIRCA), one knows that the effective permeability is nearly constant for both virgin and char at pressures over 0.2 atm. In present work, the effective permeability is expressed by void fraction in the form

$$K = C\varepsilon^n \tag{9}$$

where C is a coefficient dependent on gas pressure. When the experimental results of Marschall and Cox are fitted for pressures above 0.2 atm and the transverse and in-plane orientation values are averaged, the values of C and n are determined to be 9.78×10^{-11} m^2 and 0.381, respectively.

Diffusion

The mass flux, permeability, and pressure of the pyrolysis gas are related by the Darcy's law (see Ref. 16), which can be written in the form

$$\varepsilon\rho_g u = -\frac{K}{\mu}(\varepsilon\rho_g)\varepsilon\frac{\partial p}{\partial x} \tag{10}$$

The negative of the divergence of the right-hand side, while holding the K, μ, and $\varepsilon\rho_g$ constant, expresses the rate of change of pyrolysis gas density caused by the spatial nonuniformity in the pyrolysis gas pressure, that is, diffusion. Thus, the expression

$$D = \frac{K}{\mu}(\varepsilon\rho_g)\varepsilon\frac{\partial^2 p}{\partial x^2} \tag{11}$$

represents the diffusion term in the right-hand side of Eq. (3).

Inertial Force

Deviation from Darcy's law is observed when the velocity of the diffusing medium is high, that is, when the Reynolds number based on the pore dimensions is greater than 3 (see Refs. 7 and 16). This is due to the inertial contribution to the momentum balance. In Ref. 12, this effect is represented as the second term in the so-called Cornell–Katz equation. The coefficient of this term has never been measured for the heatshield material for the Pioneer-Venus vehicles. In the present work, the theoretical approach of

Ward[22] for rough surfaces, which is believed to be equivalent, is adopted:

$$I = 1.222\left(1/\sqrt{K}\right)\rho u^2 \tag{12}$$

Thermophysical Properties

Solid Property

The specific heat of solid carbon char was obtained from JANAF tables[23] and fitted by a curve in the form

$$c_p(T) = c_1 z^4 + c_2 z^3 + c_3 z^2 + c_4 z + c_5 \tag{13}$$

where $z = \log_{10} T$, $c_1 = -6.5$, $c_2 = -143.7$, $c_3 = 706.7$, $c_4 = 1835.0$, and $c_5 = -5700$.

Potts shows that the thermal conductivity of carbon–phenolic varies over a wide range.[24] The thermal conductivity can be expressed either in a weighted form between virgin and char or in a unified curve.[9,10,24,25] In this study, a unified curve is used to fit the experimental data given by Wakefield and Pitts,[2] in the form

$$\log_{10} \kappa(T) = aT^2 + bT + c \tag{14}$$

where $a = -6.5 \times 10^{-8}$, $b = 0.5 \times 10^{-3}$, and $c = -0.1$.

The expression for the pyrolysis rate R is obtained by modifying the expression given in Ref. 2. In Ref. 2, R is given by two different expressions below and above 622 K. These expressions do not reach zero when the resin is totally depleted. The more accurate form[9,11,24–26] producing zero value at resin depletion is

$$R = \sum_{k=1}^{N} A_k \exp\left(-\frac{B_k}{T}\right)\rho_v \left(\frac{\rho_s - \rho_c}{\rho_v}\right)^n \tag{15}$$

A two-legged expression, $N = 2$, is used here to correspond to the two-tiered expression of Ref. 2. The constant n is taken to be 2, a commonly used value.[9,11,26] The activation energy is taken also from Ref. 2 to be $B_k = 3544$ and 19,680 K for $k = 1$ and 2, respectively. The constant A is fitted to the values given by Ref. 2 at the midpoint of pyrolysis to be $A_k = 677.0$ and 1.64×10^9 s^{-1} for $k = 1$ and 2, respectively.

Pyrolysis Gas Properties

According to Ref. 2, the virgin and the char used for the Pioneer-Venus mission had a density of 1490 and 1240 kg/m^3, respectively. The elemental composition of the resin was given as C:H:O = 0.4196:0.1676:0.4128 by mass, or 1.3527:6.4457:1 by mole. The pyrolysis gas is considered here to consist of C, CH, CH_2, CH_3, CH_4, CO, CO_2, C_2, C_3, H, HO, H_2O, O, and O_2. It is assumed to be in equilibrium at the local solid temperature. The equilibrium gas properties are obtained by interpolating the equilibrium gas tables. The standard energy of formation of this gas is found to be 1.141×10^7 J/kg.

The energy of pyrolysis is reported[2] as 3.72×10^5 J/kg of virgin material. The standard energy of formation of the resin is deduced from this value, and the known formation energy of the pyrolysis gas is 2.2×10^6 J/kg.

Solution Procedure

Numerical Scheme

The four governing equations are separated into two groups, solid phase and gas phase. The two sets of equations are solved in a loosely coupled manner. For each group, integration is made fully implicitly in time. The time step chosen for the integration of the solid phase is between 0.01 and 0.1 s depending on the rate of change of the heating rate, whereas that for the gas phase is chosen between 10^{-3} and 10^{-4} s. A second-order differencing in space and a first-order differencing in time was applied to yield the implicit finite difference. Representing the equations set by

$$\frac{\partial U}{\partial t} + \frac{\partial E}{\partial x} = H \tag{16}$$

the scheme results in a difference equation of the form

$$-\frac{\Delta t}{2\Delta x}\left(\frac{\partial E}{\partial U}\right)_{j-1} \Delta U_{j-1} + \left[I - \Delta t\left(\frac{\partial H}{\partial U}\right)_j\right]\Delta U_j + \frac{\Delta t}{2\Delta x}\left(\frac{\partial E}{\partial U}\right)_{j+1} \Delta U_{j+1} = -\frac{\Delta t}{2\Delta x}(E_{j+1} - E_{j-1}) + \Delta t H_j \tag{17}$$

where the coefficients of ΔU and right-hand side are evaluated at the n-time level. The resulting algebraic equation set is solved by a block-tridiagonal matrix inversion method. A Courant–Friedrichs–Lewy (CFL) number of up to 1000 is used for the integration of the gas-phase equations. A 10–100 time step integration of the gas-phase equations enabled the gas-phase integration to catch up with the solid-phase integration.

Boundary Conditions

The boundary condition at the inner boundary is imposed as follows: The solid mass equation (2) does not require a boundary condition. For the gas mass equation (3), an equation is derived by dropping the temporal term on the left-hand side, and the diffusion term in the right-hand side specifies the boundary condition. For the momentum equation (4), the condition of zero velocity is imposed. For the energy equation (5), an adiabatic condition, that is, an insulated wall condition, is imposed.

At the outer boundary, the solid mass equation (2) is unaffected. The condition for pyrolysis gas mass, Eq. (3), is obtained from the equilibrium condition for the pyrolysis gas at the given surface pressure and temperature. For the momentum equation (4), no boundary condition is necessary at the outer boundary because the resulting ordinary differential equation is of first order in space and because one boundary condition is already imposed at the inner boundary. Finally, for the energy equation, the wall slope of temperature is specified to correspond to the given wall heat transfer rate. The boundary conditions at both boundaries are treated implicitly in time with a second-order spatial accuracy.

The developed computer code SCMA is written in the form of a subroutine. It is run in a loosely coupled manner with the trajectory calculation.

Results and Discussion

Solution of Pyrolysis Gas Flow

As already mentioned, the two sets of the governing equations are solved in a loosely coupled manner. Integration timescales applied to each set of equations are different. One timescale is for describing the change in the trajectory and, therefore, heating rate, and the other is for the CFD solution of the pyrolysis gas.

The method of solving the gas flow is the same as in standard CFD. The gas flowfield is initialized with the surface pressure in every solid-phase time step. The CFL number for the gas-phase integration is kept to 1000. Calculation of the gas phase is continued until 1) the gas-phase time step catches up with the solid-phase time or 2) the $L2$ norms of the mass and momentum equations reach 10^{-5} at the same time. The latter is reached typically after about 50 iterations for low temperature and pressure and about 500 iterations for high temperature and pressure. The computing time used is about 2×10^{-4} s per iteration and per node point in an IRIS R10000 workstation.

Arc-Jet Data by Wakefield and Pitts

The developed SCMA code was validated against the experiment conducted in an arc-jet wind tunnel by Wakefield and Pitts.[2] In the test, a carbon–phenolic test specimen was exposed to 1400 W/cm^2 of convective heat transfer rate for 5 s in an airflow. The surface pressure and flow enthalpy are given as 0.22 atm and 23,300 J/g, respectively. The nose radius is set to be 1.0 cm in this validation. This selected nose radius is consistent with the given pressure and enthalpy values. The thickness of the model is unknown and is taken to be 1 cm. The properties of the carbon–phenolic used in that experiment are the same as those used in the present work.

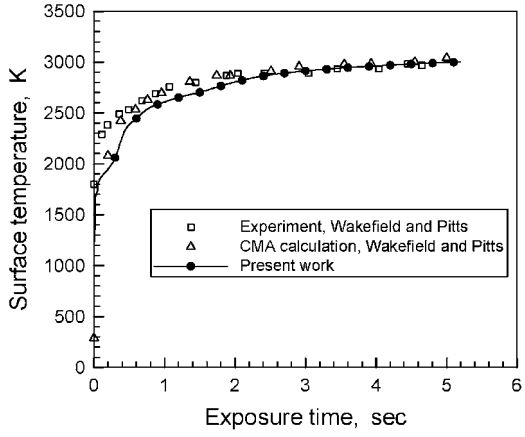

Fig. 1 Comparison between the surface temperature measured in an arc-jet experiment by Wakefield and Pitts[2] and the calculation by Wakefield and Pitts using CMA and by the present method.

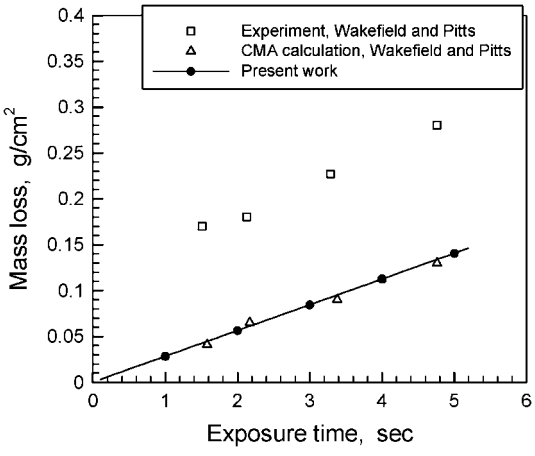

Fig. 2 Comparison between the mass loss measured in an arc-jet experiment by Wakefield and Pitts[2] and the calculation by Wakefield and Pitts using CMA and by the present method.

The heating rate value of 1400 W/cm^2 was presumed, calculated using the formula of Fay and Riddell[27] and confirmed by the use of a copper calorimeter. The true heating rate of an ablating model is different from 1400 W/cm^2 because of the surface oxidation with atomic oxygen, sublimation, convective blockage, and wall radiation. The true heating rate is calculated in the present work to be 1300 W/cm^2 initially and to decrease to the final value of about 600 W/cm^2. The calculated results of surface temperature and mass loss are compared with the experimental data and the CMA result in Figs. 1 and 2. As seen here, the present result agrees with the experiment data and with the calculation by Wakefield and Pitts[2] obtained with the CMA code. The calculated mass loss contains the influence of oxidation at surface.

Comparison with HBI Result

The SCMA code was also validated through a comparison of its solutions with HBI results.[15] The test case is a 40-s flight of a conical reentry vehicle of small cone half-angle from an altitude of 90 to 0 km. The cold wall heating rate, recovery enthalpy, and pressure are described in Table 1 in Ref. 15. The heat flux in the 0–22-s time span is for laminar flow, and that after 23 s is for turbulent flow. Figure 3 shows a comparison of the surface temperatures calculated by HBI and the present method. There are three solutions under HBI: heat balance integral–quasi-steady charring (HBI-QS), heat balance integral–generalized cubic, generalized charring (HI-Gen), and finite difference method (FDM).[15,25] In the two HBI methods, the solution is obtained by a spatial integration of temperature equation, whereas in the FDM, the solution is obtained by differencing the temperature equation. As shown in Fig. 3, the result of the present method agrees fairly well with those of HBI, except that the present peak value is slightly higher.

Table 1 Characteristics of Pioneer-Venus probe vehicles

Probe	M, kg	R_N, m	γ, deg	Entry time
Day	76.9	0.18	−25.4	1855:31.0
Night	76.9	0.18	−41.5	1859:19.2
North	76.9	0.18	−68.7	1852:52.8
Large	299.3	0.355	−32.4	1848:44.9

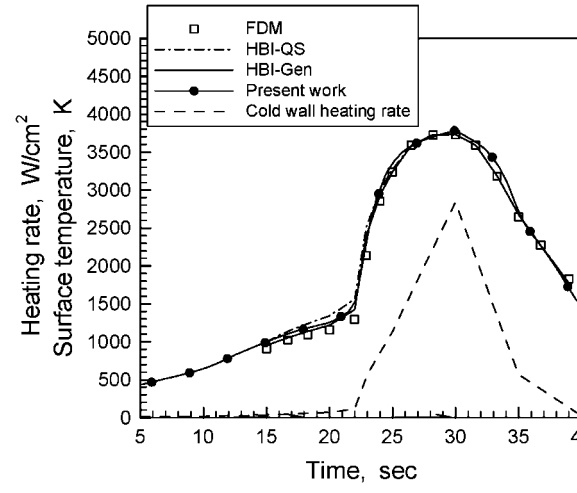

Fig. 3 Comparison between surface temperature calculated by FDM,[15] HBI method,[15] and present method.

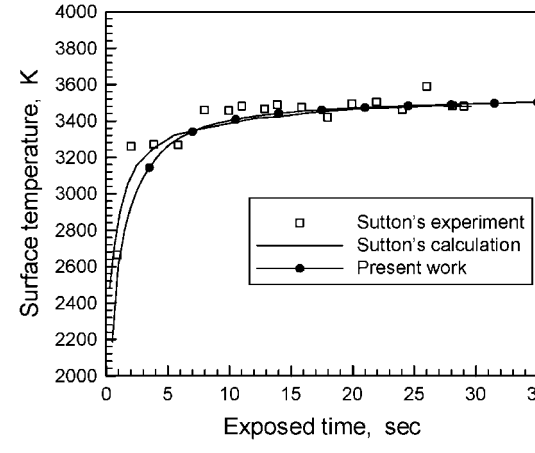

Fig. 4 Comparison between surface temperature measured and calculated by Sutton[28] and calculated by the present method.

Arc-Jet Data by Sutton

Further comparison is made with the arc-jet data obtained by Sutton.[28] In this experiment, the stagnation pressure and enthalpy were 0.31 atm and 25.05 MJ/kg. The cold-wall heat transfer rate was 14.2 MW/m^2. Calculated surface temperature values are compared with the experimental data and the calculation by Sutton in Fig. 4. As shown in Fig. 4, the present result agrees well with the experimental data and with the calculation by Sutton. The surface recession is compared in Fig. 5. As seen here, the present method also results in an excellent agreement with the experimental data for the surface recession.

Pioneer-Venus Heating Environment

The present method is used in numerically recreating the thermocouple data obtained during the flights of the four Pioneer-Venus probe vehicles.[1,2,29] The relevant characteristics of the four vehicles are presented in Table 1. All four vehicles are believed to have entered at 11.537 km/s at the altitude of 200 km. However, the times for passing the 200-km point are different, as shown in Table 1. The

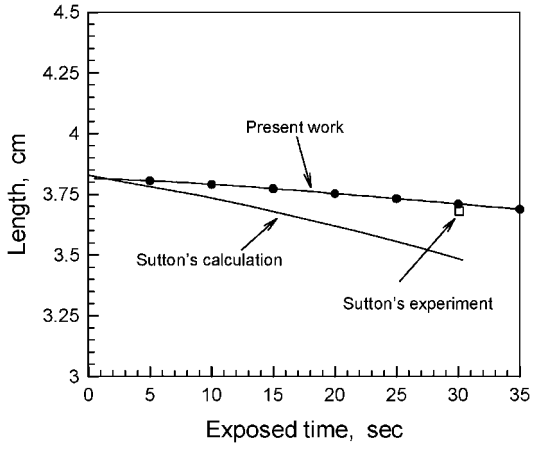

Fig. 5 Comparison between recession length measured and calculated by Sutton[28] and calculated by the present method.

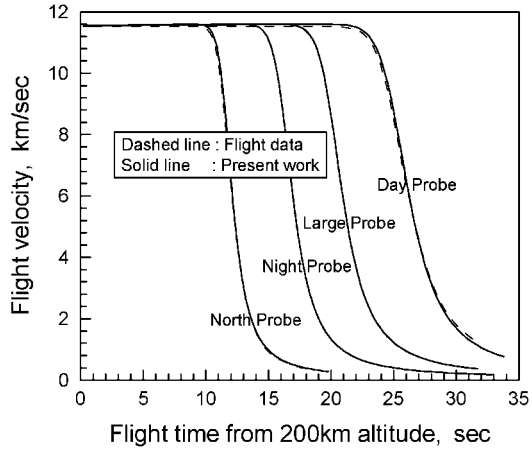

Fig. 6 Comparison between the velocity history calculated from accelerometer data[1] and present calculation for the Pioneer-Venus day and north probe.

forward thermocouples were located at $s/R_N = 0.3$ for the three small probes, slightly off the stagnation point for each of the small probes, and $s/R_N = 0$ for the large probe. They were placed 0.59 cm away from the inner boundary of the heatshield for all probes.[2] The numerical reconstruction of thermocouple temperature for these vehicles is made in the present work only for the stagnation region. This is because the turbulence characteristics affecting the heating rate at the downstream point are not known.

The convective heat flux for the stagnation region of the Pioneer-Venus probes are calculated using a viscous shock layer method by Park and Ahn.[6] In this method, finite-rate chemical reactions are assumed for both the gas phase and for gas–surface interactions. Injection of pyrolysis gas is accounted for separately from vaporization of the char surface. Radiative heating rate is calculated line-by-line, including the effect of absorption by the ablation product. This method, among others, yields the convective blockage factor in the form of an empirical curve fit.

The flight velocities of the day and north probes were deduced from the accelerometer data described in Ref. 1. The deceleration data were digitized in the flight times between 14.86 and 31.8 s for the day probe and 8.84 and 18.34 s for the north probe measured from the altitude of 200 km (see Figs. 3 and 4 in Ref. 1). The deceleration data were extrapolated linearly from $t = 0$ to the digitized times. The accelerometer data are not available for the night and large probes. Therefore, their trajectories are calculated here from the given initial altitude, velocity, and flight-path angle assuming zero angle of attack. The drag coefficient necessary for this calculation is taken from Ref. 1. In Fig. 6, the results of the trajectory calculation are compared with the flight data. For the day and north probes, the present calculation agrees well with the accelerometer data.

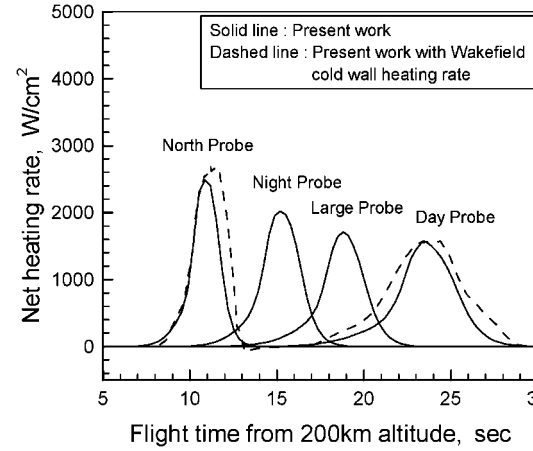

Fig. 7 Net heating rates calculated using Wakefield and Pitts cold wall heating rates and by the present work for the stagnation point of the Pioneer-Venus probes.

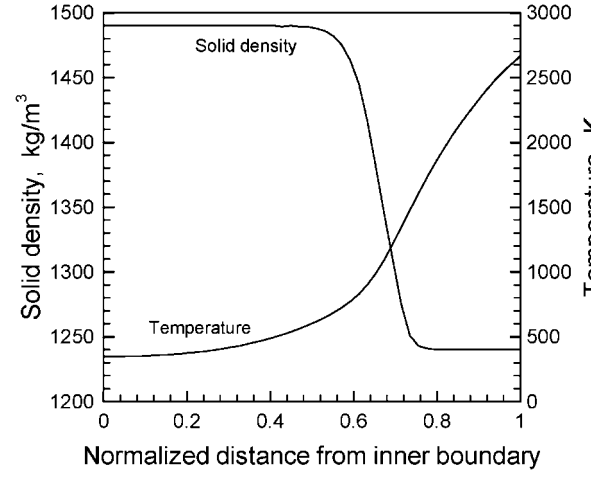

Fig. 8 Distribution of solid density and temperature within the heatshield at t = 27 s for day probe calculated by the present method.

In Fig. 7, the net heating rate values, that is, the sum of convective and radiative fluxes minus wall radiative cooling, are compared. The dashed line represents the net heating rate values calculated by the present method with the Wakefield and Pitts[2] wall heating rate. The solid line indicates the net heating rate values calculated by the present method. As seen, the present values are lower than the Wakefield and Pitts value.

Pyrolysis Gas Behavior for Pioneer-Venus

Figure 8 shows the solid density and temperature variations at $t = 27$ s for the day probe. At about $t = 27$ s, the thermocouple temperature is at its peak. Pyrolysis does not occur in the region between $X = 0$ and 0.55, and the char is formed in the range $X > 0.75$. The thickness of the pyrolysis zone is about 20% of heat shield thickness at $t = 27$ s. The temperature at the inner boundary is changed slightly from its initial value at that time. The temperature distribution has a peak curvature at about $X = 0.6$ and at $X = 0.80$. The negative curvature at $X > 0.80$ implies that the surface temperature is decreasing at this time point. The temperature at the inner wall is virtually unchanged. This means that, for this case, the boundary condition for the temperature equation at the inner boundary is immaterial.

Figure 9 shows the gas pressure inside the heatshield of the Pioneer-Venus day probe. The gas pressure rises and is nearly constant in the inner region. The region in which the pressure varies abruptly coincides with the pyrolysis zone in which the void fraction changes. Pyrolysis gas pressure reaches up to about 30 atm. Such a high internal pressure may induce spallation. Shia and McManus[30] showed that the internal gas pressure in carbon–phenolic can be high more than 30 atm.

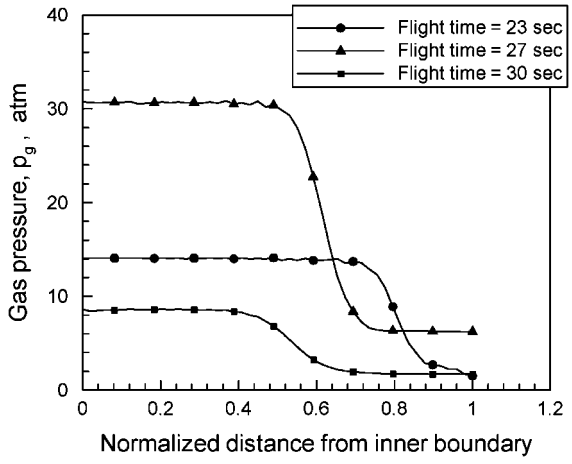

Fig. 9 Gas pressure inside heatshield of the Pioneer-Venus day probe.

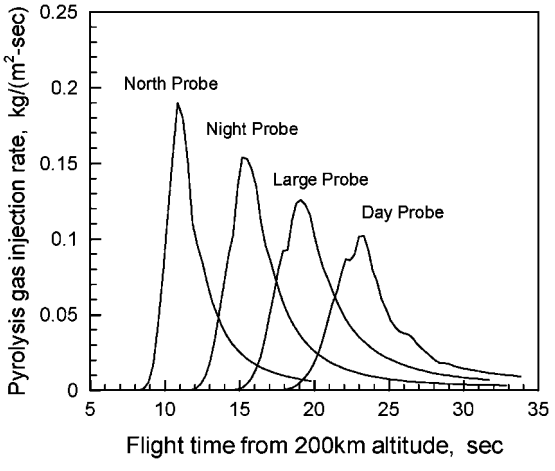

Fig. 10 Pyrolysis gas injection rates for Pioneer-Venus probes.

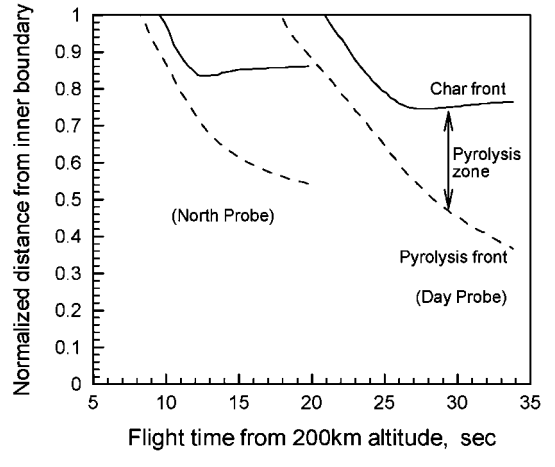

Fig. 11 Pyrolyzing behavior of the heatshield for north and day probes.

Figure 10 shows the pyrolysis gas injection rates for the four vehicles. When the pyrolysis gas injection rates calculated in the present work are integrated over the flight time and wetted surface of the four probes under the assumption of a uniform ablation rate, the mass losses by the pyrolysis gas injection are 0.616, 0.585, 0.595, and 2.2 kg for the day, night, north, and large probes, respectively.

Figure 11 shows the temporal variation of the char front and the pyrolysis front in the material for the north and day probes. The pyrolysis zone shown in Fig. 11 is defined as the zone bounded by the two limits: The lower limit is where the solid density is greater than the char density by 0.6%. The upper limit is where the solid density is lower than the virgin density by 0.6%. The pyrolysis occurs at about 8 and 18 s for the north and day probes and is followed by the charring after few seconds. The pyrolysis zone grows with time. The advancement of the char front stops when the heating pulse is over. However, the pyrolysis front continues to advance. The pyrolysis zone becomes ever wider thereafter.

Pioneer-Venus Thermocouple Data

The heating rates for the day and north probes were calculated by Wakefield and Pitts[2] using the method of Zoby et al.[4] and of Falanga and Olstad.[5] The heating rates were calculated therein[2] assuming thermochemical equilibrium and steady-state ablation. Calculation of thermocouple temperature is performed here using the present method, first using these heating rates. The results are shown in Figs. 12 and 13 and are compared with the calculation by Wakefield and Pitts.[2]

As seen in Figs. 12 and 13 and mentioned in the Introduction, the calculation by Wakefield and Pitts[2] predicted the temperatures to exceed the melting point of the thermocouples. In comparison, the present results with the same heating rates show maximum temperatures to be below the melting temperature.

The foregoing calculation was repeated with the heating rates given by Park and Ahn.[6] The calculated thermocouple temperatures are compared with the flight data for day and north probes in Figs. 12 and 13. As seen in Figs. 12 and 13, the present method based on the heating rates by Park and Ahn yields better agreement than the

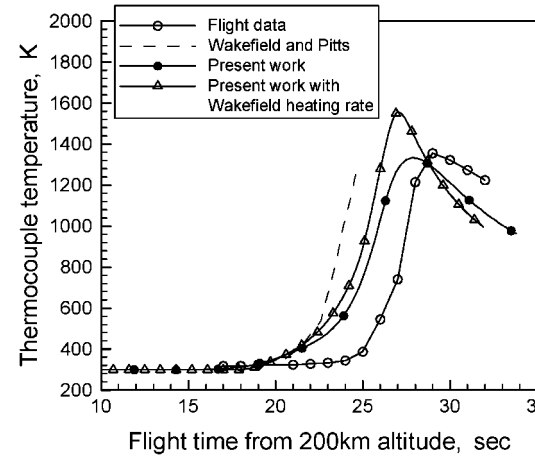

Fig. 12 Comparison between the calculated and measured temperature history for the thermocouple located 0.41 cm deep in the stagnation region of the Pioneer-Venus day probe, $\gamma = -25.4$ deg.

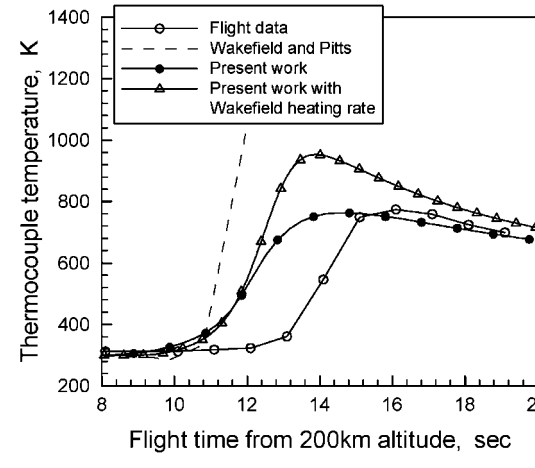

Fig. 13 Comparison between the calculated and measured temperature history for the thermocouple located 0.41 cm deep in the stagnation region of the Pioneer-Venus north probe, $\gamma = -68.7$ deg.

calculation by Wakefield and Pitts[2] or the present method using Wakefield and Pitts heating rates. In particular, the present method produces slopes and peak values closer to the flight data, although the points of onset of temperature rise do not agree with the flight data. The slope signifies the rate of energy transfer. The agreement of calculated slopes with those in-flight implies that the rate of energy transfer is correctly modeled in the present method.

For both the day probe and north probe, there is a tendency to predict the onset of thermocouple temperature rise to be earlier by about 2 s. This may be attributed to the heat transfer phenomenon occurring within and around the thermocouple junctions. Even though tests were conducted before the launch of the Pioneer-Venus mission to verify proper functioning of the thermocouples, those tests could not correctly reproduce the high and sudden heating pulses encountered in the actual entry flight into Venus. Thus, by forgiving the 2-s error in the onset of temperature rise, the present results should be viewed to be in a good agreement with the flight data.

In Figs. 14 and 15, the calculated thermocouple temperatures for night and large probes are compared with the flight data. The present results are higher than the flight data. The disagreement seen in Figs. 14 and 15 for night and large probes may be attributed to the error in the entry trajectory. As mentioned, for the night and large probes shown in Figs. 14 and 15, the accelerometer data were absent, and the flight trajectory was constructed in the present work from the entry angles assuming zero angles of attack.

There may also exist another possible reason for the discrepancy in the onset of temperature rise. In Ref. 2, it is stated that the probe passage time through 200-km altitude is not in complete agreement

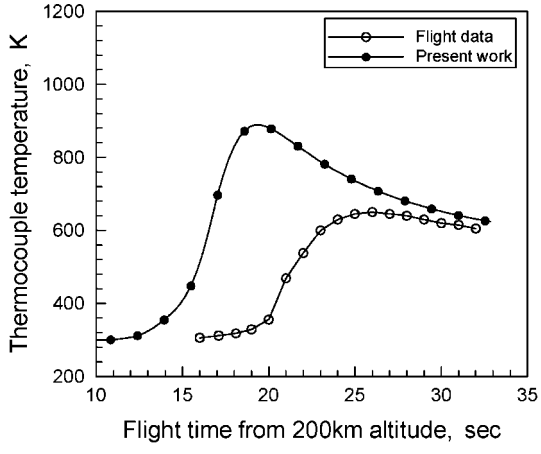

Fig. 14 Comparison between the calculated and measured temperature history for the thermocouple located 0.41 cm deep in the stagnation region of the Pioneer-Venus night probe, $\gamma = -41.5$ deg.

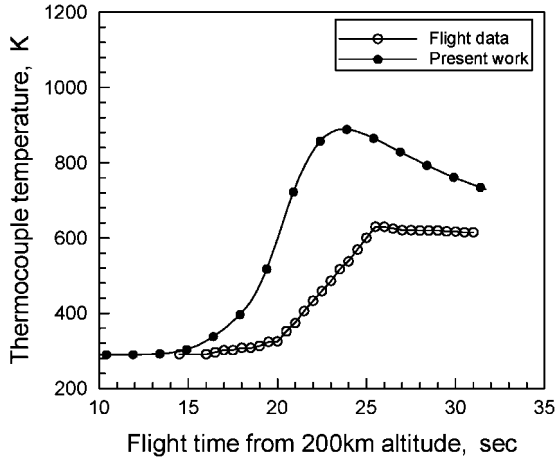

Fig. 15 Comparison between the calculated and measured temperature history for the thermocouple located 0.41 cm deep in the stagnation region of the Pioneer-Venus large probe, $\gamma = -32.4$ deg.

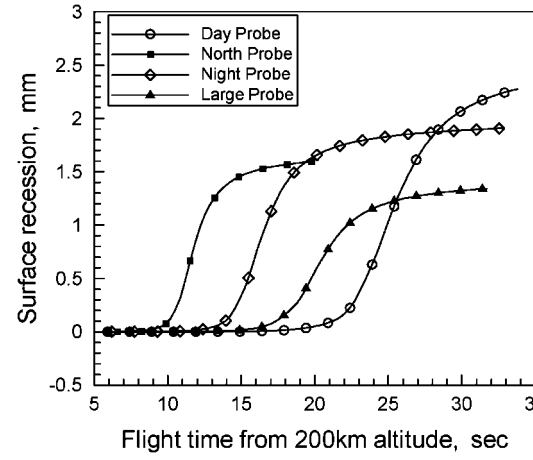

Fig. 16 Calculated surface recession for the stagnation point of Pioneer-Venus probes.

among the four vehicles. The extent of the possible clocking errors is investigated as follows. In the original data, the reference entry altitude is 200 km for all four probes. The reference entry altitude is changed arbitrarily until the calculated values agreed closest with the flight data. The changed initial entry altitudes are 210, 235, 217, and 213 km for the day, night, north, and large probes, respectively. The corresponding time discrepancies are about 0.87, 3.03, 1.47, and 1.13 s for the day, night, north, and large probes, respectively.

The calculated surface recession at the stagnation point due to vaporization is presented in Fig. 16. Of the four probes, the day probe is ablated most severely. If ablation occurred over the entire heatshield surface uniformly at the same rate as the calculated stagnation point values, then the mass loss by vaporization would be 1.5, 1.27, 1.054, and 3.6 kg for the day, night, north, and large probes, respectively, when heating is finished. The calculated total mass losses of each probe vehicle including the effect of the pyrolysis injection are 2.75, 2.41, 2.14, and 1.94% of the initial mass for the day, night, north, and large probes, respectively.

Conclusions

A computer program for the analysis of charring materials ablation, SCMA, is developed by modifying the methodology used in the existing CMA code or the HBI method to account for the unsteady motion of the pyrolysis gas, diffusion, friction, and inertial forces. The code reproduces the results obtained using CMA and other codes and the results of laboratory and flight experiments. For the day probe and north probe of the Pioneer-Venus mission, for which the entry angle and flight trajectory are known, good agreement is seen between the present calculation and the flight data. For the night probe and large probe, for which entry angle and trajectory are unknown, the calculated thermocouple temperatures are substantially higher than the flight values, and the onset of their rise is substantially earlier than the flight values.

References

[1] Seiff, A., Kirk, D. B., Young, R. E., Blanchard, R. C., Findlay, J. T., Kelly, G. M., and Sommer, S. C., "Measurement of Thermal Structure and Thermal Contrasts in the Atmosphere of Venus and Related Dynamical Observations; Results from the Four Pioneer Venus Probes," *Journal of Geophysical Research*, Vol. 85, No. A13, 1980, pp. 7903–7933.

[2] Wakefield, R. M., and Pitts, W. C., "Analysis of the Heat-Shield Experiment on the Pioneer-Venus Entry Probes," AIAA Paper 80-1494, July 1980.

[3] Kendall, R. M., Rindal, R. A., and Bartlett, E. P., "Thermochemical Ablation," AIAA Paper 65-642, June 1965.

[4] Zoby, E. V., Moss, J. N., and Sutton, K., "Approximate Convective Heating Equations for Hypersonic Flows," AIAA Paper 79-1078, June 1979.

[5] Falanga, R. A., and Olstad, W. B., "An Approximate Inviscid Radiating Flowfield Analysis for Sphere–Cone Venusian Entry Vehicles," AIAA Paper 74-758, July 1974.

[6]Park, C., and Ahn, H.-K., "Stagnation-Point Heat Transfer Rates for Pioneer-Venus Probes," *Journal of Thermophysics and Heat Transfer*, Vol. 13, No. 1, 1998, pp. 33–41.

[7]April, G. C., "Evaluation of the Energy Transfer in the Char Zone During Ablation," Ph.D. Dissertation, Dept. of Chemical Engineering, Louisiana State Univ., Baton Rouge, LA, May 1969.

[8]McManus, H. L., and Springer, G. S., "High Temperature Thermomechanical Behavior of Carbon–Phenolic and Carbon–Carbon Composites, I. Analysis," *Journal of Composite Materials*, Vol. 26, No. 2, 1992, pp. 206–229.

[9]Clever, R. M., and Denny, V. E., "Response of Charring Ablators to Severe Aerodynamic and Erosion Environments," *Journal of Spacecraft and Rockets*, Vol. 12, No. 9, 1975, pp. 558–564.

[10]Chang, C. I., Griffs, C. A., Stonesifer, F. R., and Nemes, J. A., "Thermomechanical Effects of Intense Thermal Heating on Materials/Structures," *Journal of Thermophysics and Heat Transfer*, Vol. 1, No. 2, 1987, pp. 175–181.

[11]Bueche, J. F., "Effect of Improvements and Uncertainties in Thermophysical Properties on Carbon Phenolic Heatshield Thermal Performance Predictions," AIAA Paper 77-787, June 1977.

[12]Smyly, E. D., Swoger, W. F., and Pears, C. D., "Thermal and Mechanical Properties of Low-Density Phenolic-Nylon and Silicone-Phenolic Ablators," NASA CR-111909, June 1971.

[13]McManus, H. L., and Springer, G. S., "High Temperature Thermomechanical Behavior of Carbon–Phenolic and Carbon–Carbon Composites, II. Results," *Journal of Composite Materials*, Vol. 26, No. 2, 1992, pp. 230–255.

[14]Marschall, J., and Cox, M. E., "Gas Permeability of Lightweight Ceramic Ablators," *Journal of Thermophysics and Heat Transfer*, Vol. 13, No. 3, 1999, pp. 382–384.

[15]Leone, S. A., Potts, R. L., and Laganelli, A. L., "Enhancements to Integral Solutions to Ablation and Charring," *Journal of Spacecraft and Rockets*, Vol. 32, No. 2, 1995, pp. 210–216.

[16]Kaviany, M., *Principles of Heat Transfer in Porous Media*, 2nd ed., Springer, New York, 1995, pp. 18–48.

[17]Park, C., Jaffe, R. L., and Partridge, H., "Chemical-Kinetic Parameters of Hyperbolic Earth Entry," *Journal of Thermophysics and Heat Transfer*, Vol. 15, No. 1, 2001, pp. 76–90.

[18]Park, C., *Nonequilibrium Hypersonic Aerothermodynamics*, Wiley, New York, 1990, pp. 129–133.

[19]Biolsi, L., and Flori, B., "Transport Properties Associated with Entry into the Atmosphere of Titan," AIAA Paper 81-0278, Jan. 1981.

[20]Wilke, C. R., "A Viscosity Equation for Gas Mixtures," *Journal of Chemical Physics*, Vol. 18, No. 4, 1950, pp. 517–519.

[21]Marschall, J., and Milos, F. S., "Gas Permeability of Rigid Fibrous Refractory Insulations," *Journal of Thermophysics and Heat Transfer*, Vol. 12, No. 4, 1998, pp. 528–535.

[22]Ward, J. C., "Turbulent Flow in Porous Media," *Journal of the Hydraulics Division, ASCE*, Vol. 90, No. HY-5, 1964, pp. 1–12.

[23]Chase, M. W., Jr., Davies, C. A., Downey, J. R., Jr., Frurip, D. J., McDonald, R. A., and Syverud, A. N., "JANAF Thermochemical Tables, Third Edition, Parts 1 and 2," *Journal of Physical and Chemical Reference Data*, Vol. 14, Supplement No. 1, 1985.

[24]Potts, R. L., "Application of Integral Methods to Ablation Charring Erosion, A Review," *Journal of Spacecraft and Rockets*, Vol. 32, No. 2, 1995, pp. 200–209.

[25]Potts, R. L., "Hybrid Integral/Quasi-Steady Solution of Charring Ablation," AIAA Paper 90-1677, June 1990.

[26]Shaw, T. E., Garner, D. C., and Florence, D. E., "Effects of Uncertainties in Thermophysical Properties on Ablation Efficiency," *Thermophysics and Temperature Control of Spacecraft and Entry Vehicles*, edited by G. B. Heller, Vol. 18, Progress in Astronautics and Aeronautics, Academic Press, New York, 1966, pp. 513–548.

[27]Fay, J. A., and Riddell, F. R., "Theory of Stagnation Point Heat Transfer in Dissociated Air," *Journal of the Aeronautical Sciences*, Vol. 25, No. 2, 1958, pp. 73–85.

[28]Sutton, K., "An Experimental Study of a Carbon–Phenolic Ablation Material," NASA TN D-5930, Sept. 1970.

[29]Colin, L., "The Pioneer Venus Program," *Journal of Geophysical Research*, Vol. 85, No. A13, 1980, pp. 7575–7598.

[30]Shia, D., and McManus, H. L., "Modeling of Composite Ablators Using Massively Parallel Computers," AIAA Paper 95-1374, 1995.